Geophys. J. Int. (1999) **138,** 366–380

The effects of the theoretical formalism and data selection on mantle models derived from waveform tomography

Charles Mégnin and Barbara Romanowicz

Berkeley Seismological Laboratory and Department of Geology and Geophysics, University of California, Berkeley, CA 94720, *USA.*
E-mail: pepe@seismo.berkeley.edu

Accepted 1999 February 23. Received 1999 February 19; in original form 1998 May 4

SUMMARY

Most global tomographic models to date are derived using a combination of surface wave (or normal-mode) data and body wave traveltime data. The traveltime approach limits the number of phases available for inversion by requiring them to be isolated on the seismogram. This may ultimately result in limiting the resolution of 3-D structure, at least in some depth ranges in the mantle. In a previous study, we successfully derived a degree 12 whole-mantle *SH*-velocity tomographic model (SAW12D) using exclusively waveform data. In that inversion, a normal-mode formalism suitable for body waveforms, the non-linear asymptotic coupling theory (NACT), was combined with a body wave windowing scheme, referred to as the 'individual wavepacket' (IW) technique, which allows one to assign individual weights to different body wave energy packets. We here compare the relative merits of this choice of theoretical formalism and windowing scheme at different depth ranges in the mantle. Choosing as the reference a model obtained using 7500 transverse-component body wave and 8000 surface wave seismograms and the NACT and IW approaches, we discuss the relative performance of the path average approximation (PAVA), a zeroth-order theoretical approximation appropriate for single-mode surface waves, relative to NACT, and compare the IW windowing scheme with a more standard 'full window' (FW) approach, in which a single time window is considered from the first body wave arrival to the fundamental-mode surface waves. The combination PAVA/FW is often used in global tomography to supplement the traveltime data.

We show that although the quality of the image derived under the PAVA/FW formalism is very similar to that derived under NACT/IW in the first 300 km of the upper mantle, where the resolution is dominated by surface waves, it deteriorates at greater depths. Images of the lower mantle are shown to be strongly sensitive to the theoretical formalism. In contrast, the resolution of structure near the core–mantle boundary depends mostly on the windowing scheme. This is because this resolution is controlled by low-amplitude phases such as S_{diff}, which are downweighted in the FW scheme. Whilst the image obtained in D″ using the combination NACT/IW is in good agreement with images obtained by other authors using both waveforms and traveltimes, we show that, when using FW, uppermost mantle structure can be mapped into D″. This result is confirmed by synthetic tests performed on a composite of the upper-mantle geodynamic model 3SMAC. We also show, based on synthetic tests, that for structures in the upper mantle with sharp boundaries, differences are observed between NACT and PAVA. Whilst a combination of traveltimes and surface wave data is adequate for resolving relatively smooth features in the mantle, our results show that by potentially increasing the achievable sampling, the waveform approach shows great promise for future high-resolution tomographic modelling of mantle structure, if cast in an appropriate theoretical framework.

Key words: Earth's interior, global seismology, mantle, mode coupling, synthetic waveforms, tomography.

INTRODUCTION

Waveform tomography is promising for the resolution of detailed structure in the Earth's mantle in that it provides the means to utilize all of the information in the seismogram, rather than being limited to isolated phases as is the case in traveltime tomography.

Synthetic seismogram computations are generally performed in a normal-mode framework. The theoretical formalism involved in the exact modelling of a waveform through an arbitrarily heterogeneous medium is complex and the computation time prohibitive in the context of most computational environments (e.g. Lognonné & Romanowicz 1990; Geller & Takeuchi 1995). Various simplifications thus need to be made to render the problem tractable. In the last 15 years, several seismic waveform modelling techniques have been developed with the purpose of computing 3-D models of seismic wave velocity in the Earth in a reasonable time frame. The nature of the approximation used as well as the way in which the individual phases are weighted can have a significant impact on our ability to image heterogeneity.

Most global waveform tomographic studies rely on a zeroth-order asymptotic expansion, the 'path average approximation' (PAVA) (Jordan 1978; Woodhouse & Dziewonski 1984). Under PAVA, sensitivity of the waveform is restricted to the horizontally averaged structure between the source and the receiver in the vertical plane containing the great-circle path. The path average phase perturbation is expressed as the average along the ray path of the local frequencies $\delta\omega^k_{\rm local}$ as defined by Jordan (1978). To zeroth order in ℓ (where ℓ is the angular degree of the mode), PAVA is equivalent to taking into account the coupling of multiplets along a dispersion branch (Mochizuki 1986; Park 1987; Romanowicz 1987), an approximation which is reasonably accurate for surface waves. Because it offers the important advantage of being relatively fast computationally, PAVA has also been applied to the modelling of body waves, although it is not able to reproduce the 'ray' character of the path. In tomographic applications, it has been used to compute several mantle models (e.g. Woodhouse & Dziewonski 1984; Tanimoto 1990) and has been augmented with traveltime data in more recent models, under the infinite-frequency ray theory approximation (e.g. Su *et al.* 1994; Liu & Dziewonski 1994) in order to improve resolution in the lower mantle.

To account correctly for the sensitivity of broad-band body waves to the 3-D structure along the ray path it is necessary to include the effect of coupling across mode branches in the mode summation (e.g. Romanowicz 1987; Li & Tanimoto 1993). In the non-linear asymptotic coupling theory formalism (NACT) (Li & Romanowicz 1995), only the term corresponding to across-branch coupling is linearized under the assumption of smoothness of heterogeneity. The path average contribution to the seismogram remains non-linear, which improves the validity of the approach beyond the strictly short-time approximation of Li & Tanimoto (1993). To order zero in the asymptotic formalism, off-plane effects, that is, focusing and defocusing of energy affecting wave amplitudes (Romanowicz 1987), are not accounted for. Inclusion of such effects has been discussed by e.g. Clévédé & Lognonné (1996) and Marquering *et al.* (1998).

The whole-mantle shear velocity model SAW12D (Li & Romanowicz 1996) has been developed in the NACT framework. Comparisons of 'checkerboard' tests have shown increased resolution in the lower mantle over models derived under the PAVA formalism (Li & Romanowicz 1995). SAW12D also shows good agreement with the results of local modelling of heterogeneity in the lowermost mantle (Bréger *et al.* 1998).

In addition to an improved theoretical formalism, SAW12D was developed using a windowing scheme which we call the 'individual wavepacket' (IW) technique, designed to allow relative weighting of individual energy wavepackets. The IW windowing consists of extracting separately the individual body wave energy packets in each seismic trace (Fig. 1, bottom). A data weighting scheme that normalizes the individual wavepacket amplitudes enhances the signal from the low-amplitude arrivals, and simultaneously allows each waveform to be fitted independently. This method contrasts with the traditional approach where a single wavepacket consisting of a continuous train of phases starting with the first energy arrival above the noise level (Fig. 1, top) is extracted. We refer here to this windowing scheme as the 'full waveform' (FW) technique. This procedure is widespread (e.g. Tanimoto 1990; Su *et al.* 1994) and has the advantage of allowing the rapid acquisition of a large quantity of data. However, the resulting models are influenced mostly by the information contained in the high-amplitude phases, at the detriment of low-energy wavepackets such as, for example, the $S_{\rm diff}$ diffracted along the core–mantle boundary. This is because in minimizing the difference between the data and the corresponding synthetics, the inversion will preferentially satisfy the constraints imposed by the high-amplitude part of the wavepacket.

The IW method requires considerably more processing effort than the FW approach but it is crucial for the extraction of information related to the structure located in the lowermost part of the mantle, as the low-amplitude $S_{\rm diff}$ phase is arguably the most valuable source of information relative to D″ heterogeneity in a transverse-component seismogram. Since low-amplitude signal is enhanced in this method, it has the potential to increase the effect of noise. However, our data selection is entirely manual. For each deconvolved and filtered seismogram, we compute the corresponding synthetic in the reference PREM model and compare it to the observed one, both visually and using a variance reduction criterion for each wavepacket considered. In this fashion, noisy data are readily rejected as well as records affected by timing errors and errors in instrument corrections.

The issue we wish to address here is the relative benefit of the theoretical improvements of NACT over PAVA and the windowing of individual energy wavepackets versus considering the body wave part of the seismogram as a whole. To quantify these benefits, we compare four tomographic models resulting from the inversion of a data set under PAVA and NACT formalisms making use of the FW and IW windowing schemes. Ideally, one would want to use as reference a model obtained with a more exact theoretical formalism (i.e. Lognonné & Romanowicz 1990; Geller & Takeuchi 1995; Friederich 1998). However, computations for a degree-12 whole-mantle model, the number of paths considered in our study and the necessary bandwidth (down to periods of 32 s) are currently beyond reach. We therefore use as a reference the NACT-IW model, as it is the one derived with the most 'exact' theoretical formalism and the most sophisticated procedure that we can currently afford. We then observe

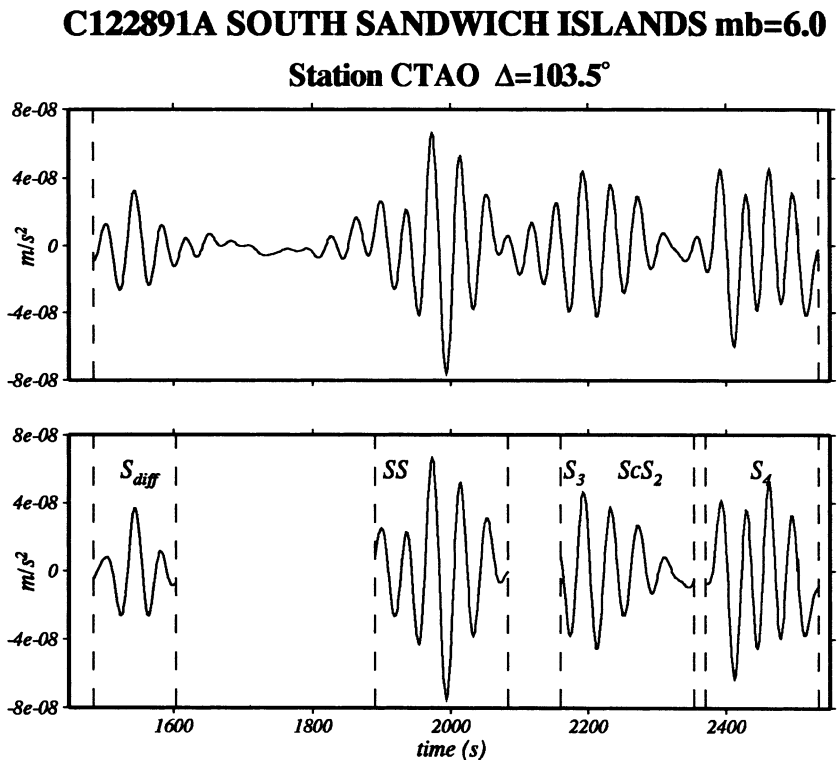

Figure 1. Top trace: full-waveform selection scheme (FW). The entire body wave train is selected. High-amplitude phases are preferentially fitted in the inversion. Bottom trace: individual wavepacket selection scheme (IW). The different energy wavepackets are selected and fitted separately. The body waveforms selected for the inversion are the energy arrivals between the dashed vertical lines. The assignment of phase names to the extracted window is not required by the theory but is used in the weighting scheme to penalize redundant paths.

and quantify how the image changes as a result of the use of a different windowing scheme (FW), a less accurate theoretical formalism (PAVA), and both. Whilst we cannot prove rigorously that the NACT-IW approach is the 'best' possible one, differences in the models can help us to gain insight into the relative importance of various inversion ingredients in different depth ranges in the mantle. In addition, resolution tests for up to degrees 8 (Li & Romanowicz 1995, Figs 5 and 6) and 12 (Li & Romanowicz 1995, Fig. 6) constitute further evidence that NACT resolves the lower mantle better than PAVA.

Inversion

We use the same inversion procedure as that used by Li & Romanowicz (1996). A detailed description is given in that paper and we present here a synopsis of its most relevant aspects.

The inverse problem is solved by making use of a stochastic formulation (e.g. Jackson 1979; Tarantola & Valette 1982) and the finite-dimensional model is obtained by the recursive application of a Newton scheme to the Fréchet derivatives of the L^2-norm objective function. The *a priori* conditions imposed through the model covariance matrix have been kept identical in the derivation of each of the four solutions. The models are expressed as relative perturbations in shear wave velocity $\delta \ln(V_{SH})$ from the spherically symmetric model PREM (Dziewonski & Anderson 1981) and are parametrized laterally in spherical harmonics up to degree 12 and radially in Legendre polynomials up to degree 5 in the upper mantle and up to degree 7 in the lower mantle.

The data are weighted by three factors: ω_e, ω_n and ω_r. Each wavepacket is scaled by $\omega \equiv \omega_e \omega_n \omega_r$. The weight ω_e corresponds to systematic error (uncertainty in source parameters, off-great-circle effects, small-scale heterogeneity, etc.) which is scaled to the amplitude of the wavepacket such that $\omega_e = 1/\epsilon$, where ϵ is the rms of the wavepacket. The weight ω_n accounts for the redundancy in the data that constitutes a given wavepacket and is computed as the geometric average of the two extremes: for no redundancy in the wavepacket, ω_n should be set to unity. In contrast, for totally redundant data, ω_n should be $1/n$, where n is the number of data points in the wavepacket. We thus set $\omega_n \equiv n^{-1/2}$. Finally, a factor ω_r accounts for the redundancy amongst wavepackets. A full description of its computation is given in Li & Romanowicz (1996), Appendix A.

Hereafter, we use the nomenclature given in Table 1 to refer to the four combinations of models derived. Horizontal comparisons (i.e. between models 1 and 2 or 3 and 4) provide information on the incidence of the theoretical formalism on the models. In contrast, vertical comparisons (i.e. between models 1 and 3 or 2 and 4) show the impact of the windowing scheme.

Table 1. Nomenclature of the four models computed in this study.

Data selection scheme/theory	NACT	PAVA
Individual wavepacket (IW)	1	2
Full waveform (FW)	3	4

Data set

We use a set of transverse-component accelerograms, consisting of 7527 body wave traces low-pass filtered at 32 s and 7919 first- and second-orbit Love wave trains low-pass filtered at 80 s collected from the GSN, GDSN and GEOSCOPE networks between 1977 and 1992. The same data set has been used in the computation of models 1 to 4.

RESULTS

In Fig. 2, we show the correlation as a function of depth of model 1 with the models resulting from each of the other three inversions. The solid line (labelled 2) represents the correlation between the NACT and PAVA formalisms. The dashed line (labelled 3) shows the correlation between IW- and FW-derived models under the NACT formalism. The dotted line (labelled 4) shows the decorrelation due to the combined use of the PAVA formalism and the FW scheme.

Uppermost mantle

In the uppermost 300 km of the mantle, models 2 and 3 remain very similar to NACT-IW (Fig. 2). A comparison between the heterogeneity patterns at 150 km [Fig. 3 (top) and Table 2(a)] shows nearly perfect correlation amongst models at that depth: in all cases, the major global tectonic features are

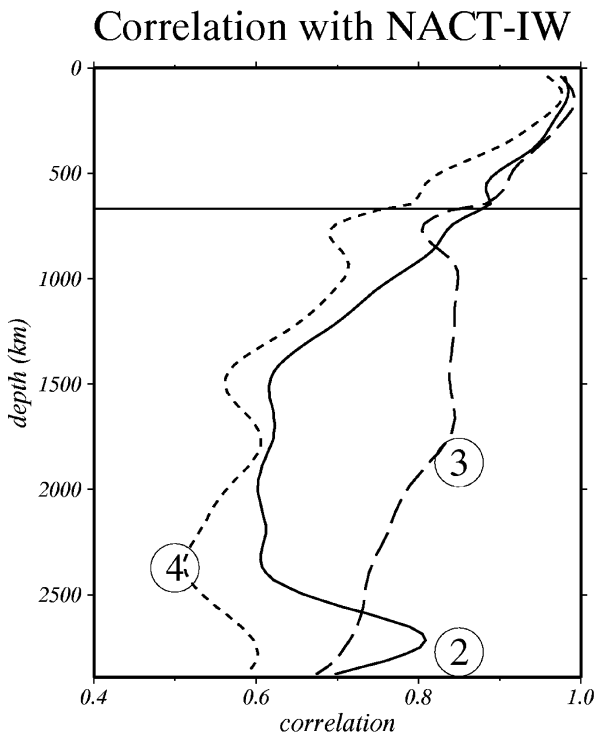

Figure 2. Correlation of the NACT-IW model with PAVA-IW (solid line), NACT-FW (dashed line) and PAVA-FW (dotted line). The model numbers correspond to those of Table 1.

Table 2. (a) Correlation between models at 150 km depth. As seen in the corresponding Fig. 3 (top), the models do not depend on which theoretical formalism and data selection scheme are used. (b) Correlation between models at 600 km depth. Theory and windowing contribute equally to the image quality. (b) corresponds to Fig. 3 (bottom). (c) Correlation between models at 1500 km depth. The decorrelation due to the use of PAVA exceeds that due to FW. (c) corresponds to Fig. 4 (top). (d) Correlation between models at 2800 km depth. Although the windowing is the most important factor, the theoretical framework contributes significantly to the image quality. The models are also correlated with the structure at 150 km depth. The FW models at the CMB correlate better with the surface heterogeneity than they do with their IW counterparts at the CMB. (d) corresponds to Fig. 4 (bottom).

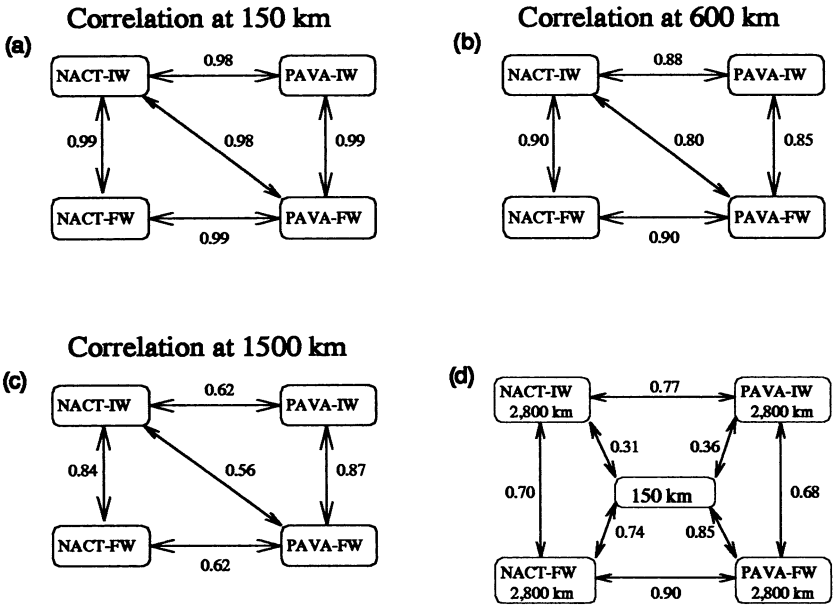

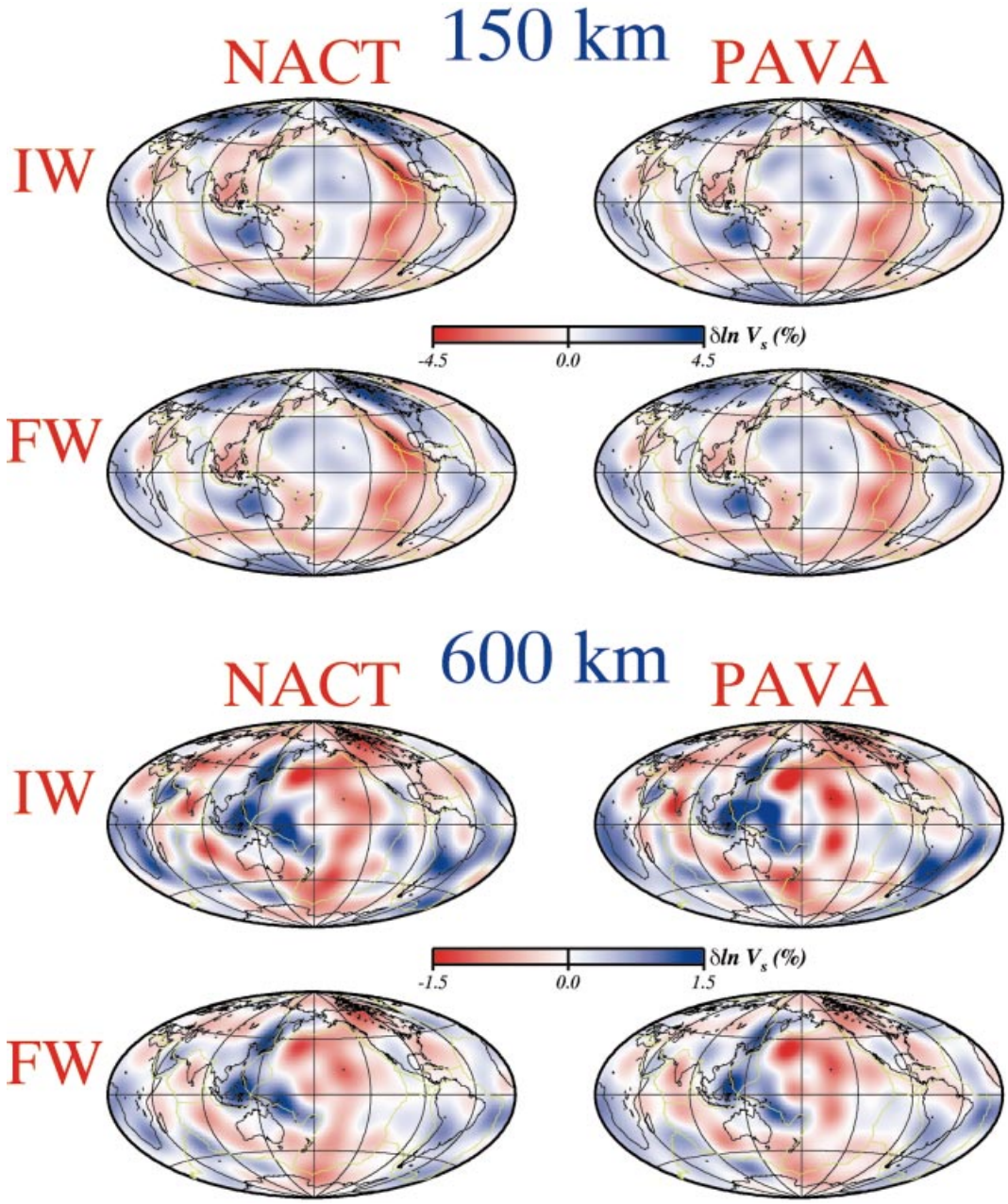

Figure 3. Top: heterogeneity at 150 km depth derived from each waveform inversion technique. The structure is sampled predominantly by surface waves and no significant difference is observed amongst the various models. Bottom: heterogeneity at 600 km depth derived from each waveform inversion technique.

well recovered. The uppermost 300 km of the mantle is predominantly sampled by Love wave trains, for which the PAVA approximation works well, as discussed above. Since the difference between IW and FW schemes applies predominantly to the modelling of body waveforms, the windowing scheme shows little impact on the tomographic image of the uppermost mantle. The similarity amongst these four images also indicates that the sets of damping parameters used in each inversion have been comparably calibrated. Except for smoothness across the 670 km discontinuity, the differences amongst the models at depths other than the uppermost mantle are unlikely to be caused by inconsistencies in the *a priori* conditions imposed to regulate the inversion. We address the issue of the smoothness constraint between the upper and lower mantle below.

Transition zone

The similarity between models decreases continuously below a depth of 300 km. In the lower part of the upper mantle, models 2 and 3 remain correlated with model 1 at the 0.90 level but the effect of the adoption of PAVA combined with FW brings the correlation between models 1 and 4 below 0.80 at the bottom of the transition zone (Fig. 2). The near-overlap between the correlation profiles of models 2 and 3 indicates that the theoretical formalism and windowing scheme in the upper mantle contribute equally to the quality of the tomographic image. In Fig. 3 (bottom) and Table 2(b), we compare the models at 600 km depth. Important features such as the westward shift with depth of low velocities in the Central

Pacific (e.g. Romanowicz *et al.* 1987) are present in all four models. However, the model details are somewhat displaced in the PAVA images, in particular under the Southern Pacific and the South American craton, and the amplitudes are decreased in the FW-derived models. The issue of model amplitude is closely related to damping in the inversion. Our experience is that slight adjustment of the damping to obtain a closer match of the amplitudes in different models is always possible. However, it will not affect the geographical distribution of model heterogeneity.

Lower mantle

In the lower mantle, the progressive decorrelation between models 1 and 2 (Fig. 2) illustrates the importance of an accurate theoretical formalism in a region sampled predominantly by large-amplitude body wave phases such as *S* and its multiples down to 2500 km depth. Fig. 4 (top) shows maps of heterogeneity at a depth of 1500 km, where models 1 and 2 are least similar. Differences in amplitudes are observed under the Asian continent, and the models differ most in

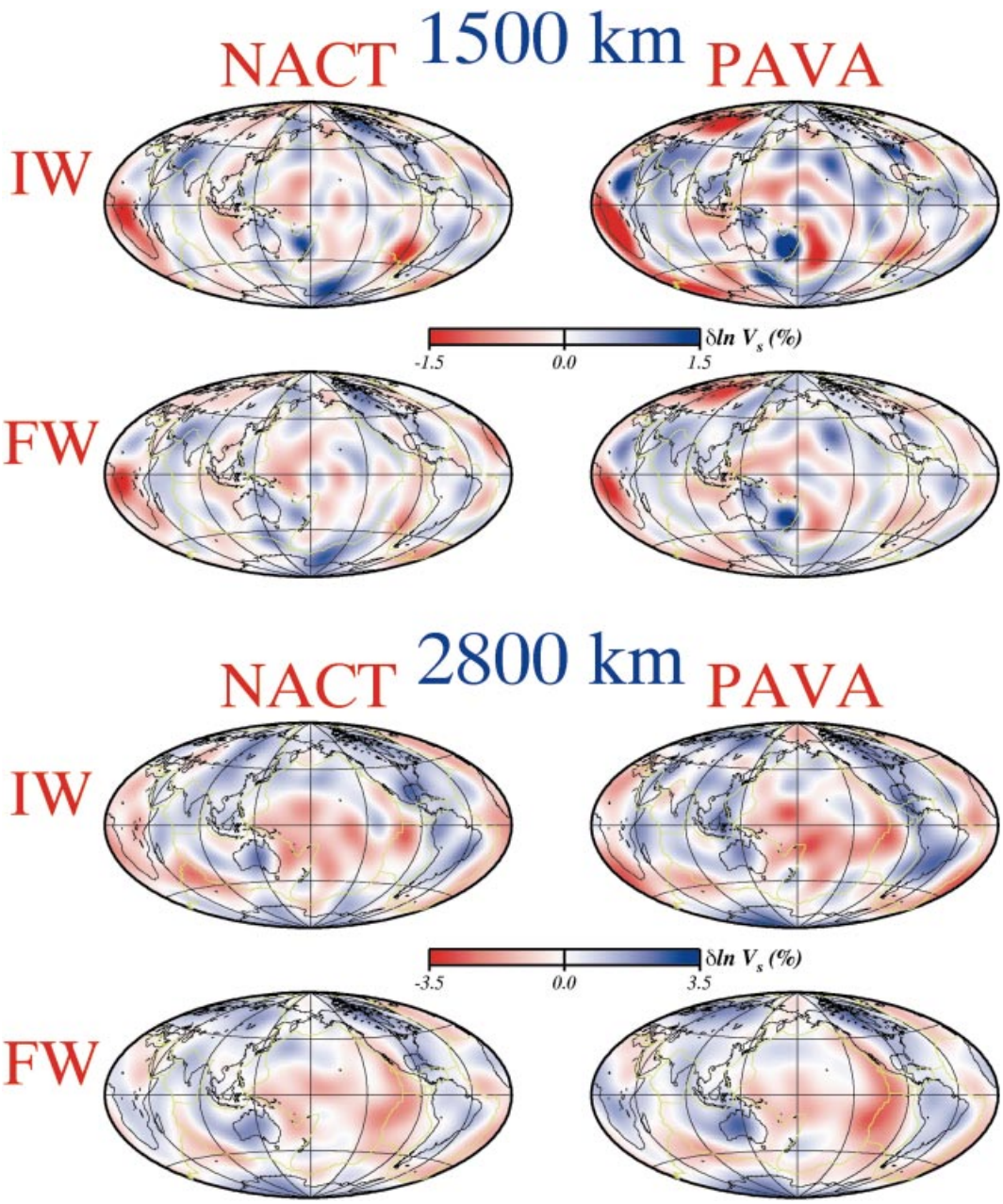

Figure 4. Top: heterogeneity at 1500 km depth derived from each waveform inversion technique. This region is predominantly sampled by large-amplitude body waves (*S*, *SS*, etc.). The quality of the image at this depth is strongly dependent on the accuracy of the waveform modelling and weakly dependent on the type of windowing scheme. Bottom: heterogeneity at 2800 km depth derived from each waveform inversion technique. The use of a non-selective windowing scheme causes the mapping of surface heterogeneity at the CMB.

pattern under the Arctic, the Central and Northeastern Pacific, the Southwestern Atlantic and the North and South American cratons. The same discrepancies persist when comparing the FW models 3 and 4, providing further evidence that the theory controls the resolution of structure in the lower mantle. Comparison between the end-member models 1 and 4 shows disagreement in most regions of the globe, with the correlation falling to 0.50 at 2300 km. In most of the lower mantle the choice of windowing has minor importance (see the similarity in correlation level between models 2 and 4 between 1000 and 2500 km depth). The decorrelation from IW-NACT to FW-NACT (or IW-PAVA to FW-PAVA) is indeed small compared to that resulting from the passage from IW-NACT to IW-PAVA (see Table 2c).

D″ region

In the lowermost mantle, the resolution is driven by the fit to the *ScS* phase and its multiples reflected on the core–mantle boundary, and the low-amplitude S_{diff} phase. In Fig. 5, we show a projection on the CMB of the coverage by 954 S_{diff}, 3766 *ScS*, 1539 ScS_2 and 125 ScS_3 phases. The linear features represent the sampling by S_{diff} and the circles correspond to the CMB reflections of *ScS* and its multiples. This projection is calculated in the ray theoretic approximation (no Fresnel zone is computed) and thus represents a lower bound of our D″ coverage. Due to inhomogeneous sampling, the Northern Hemisphere is expected to be better resolved than the Southern Hemisphere.

As discussed above, resolution at these depths is expected to be highly sensitive to the windowing scheme because of the relatively low amplitude of S_{diff}. Fig. 4 (bottom) shows considerable differences between models obtained using the two different windowing schemes, with the correlation coefficient falling below 0.70 (see Table 2d). A noticeable distortion arising from the use of FW is the change in sign of the anomaly under the Southern African craton, present in both the NACT and the PAVA models. More importantly, the D″ structure in the models derived with FW is found to be correlated up to the 0.85 level with that of the heterogeneity at 150 km depth in the NACT-IW model. Table 2(d) also shows that the FW models in the D″ region correlate better with the heterogeneity at 150 km (correlation coefficient of 0.80) than with their IW counterparts in the D″ region (correlation coefficient of 0.70). This effect is absent in the models derived with the IW scheme, where little correlation is observed between the uppermost mantle and the D″ region (correlation coefficient of 0.33). In Fig. 6, we show the spherical harmonic degree-by-degree correlation between uppermost mantle and D″ heterogeneity for all models. Models derived with the IW scheme in the NACT (solid line, diamonds) and PAVA (dashed line, circles) formalisms are poorly correlated with the surface at all degrees (correlation coefficient between 0 and 0.60), except at degree 1. On the other hand, the models derived with the FW scheme (dotted line, squares for NACT and long dashed line, triangles for PAVA) correlate strongly except at degrees 2 and 3, in particular at degrees 4 to 6, which correspond to the spectral signature of tectonics.

Our results show that upper-mantle structure is being mapped into the lower mantle at degrees higher than 3 when the FW formalism is used. This effect can be understood in the following way: lateral heterogeneity is strongest in the uppermost 200 km of the mantle, and the least-squares inversion procedure (L^2 norm constraint in the inversion) will have a tendency to map the unexplained part of the signal into the least sampled regions of the model. This is possible because although the parametrization is split across the 670 km discontinuity, imposition of a smoothness constraint between the upper and lower mantle is necessary to maintain continuity in the model rms. We indeed observe wide fluctuations in transition zone and uppermost lower mantle amplitudes

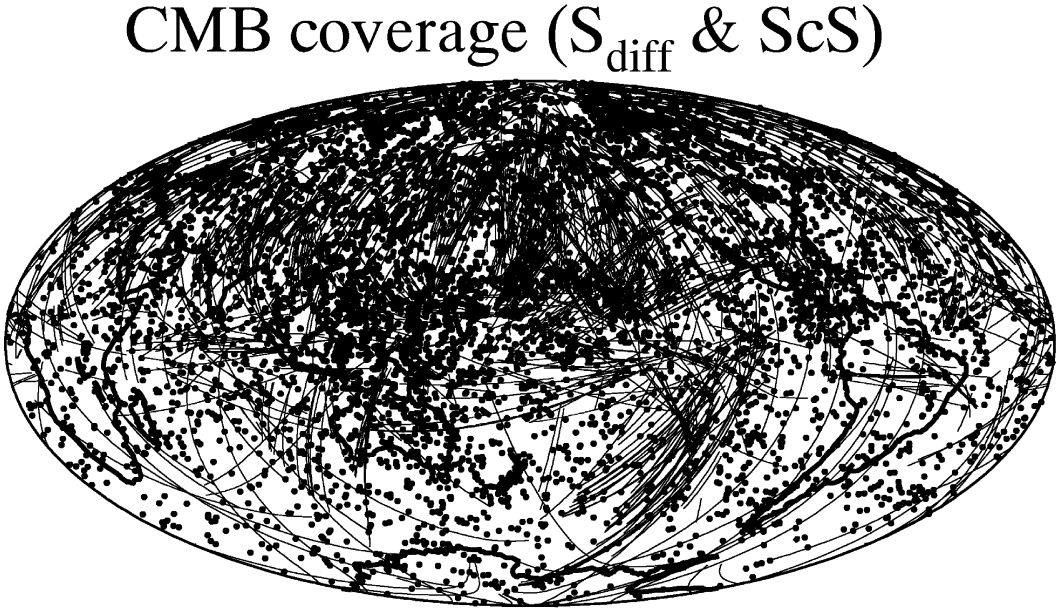

Figure 5. Coverage at the core–mantle boundary. The linear features represent the regions sampled by the 950 S_{diff} phases. The circles correspond to the 7200 CMB reflections of the *ScS*, ScS_2 and ScS_3 phases.

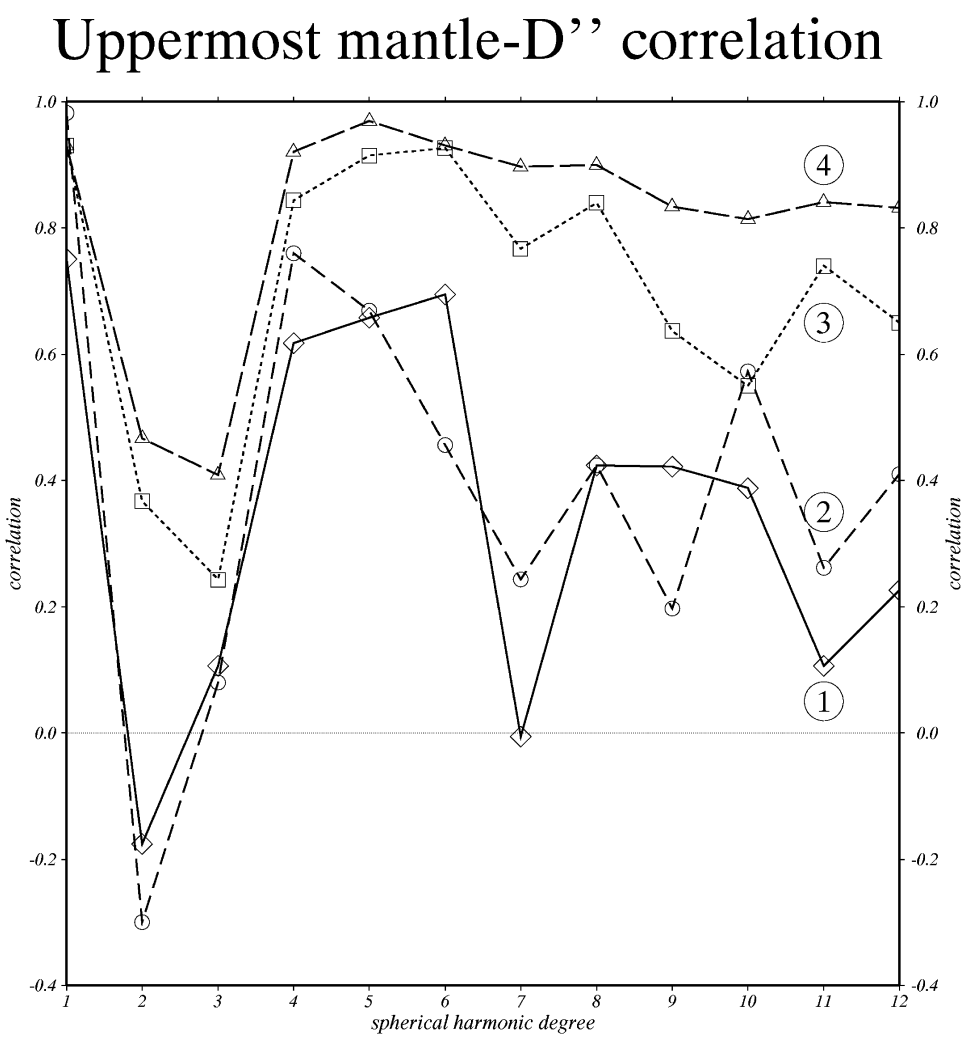

Figure 6. Degree-by-degree correlation between surface (150 km) and D″ (2800 km) heterogeneity at each spherical harmonic degree for NACT-IW (solid lines, diamonds), PAVA-IW (dashed lines, circles), NACT-FW (dotted lines, squares) and PAVA-FW (long dashed lines, triangles).

in the absence of smoothness constraints at the discontinuity. A similar trade-off would of course also be observed for a 'whole-mantle' radial parametrization, using either local or global basis functions, in the presence of radial damping.

It thus appears that in the absence of S_{diff} coverage the lowermost mantle is poorly sampled and acts as a repository for model null space. To verify that this is indeed the case, we conducted an IW-PAVA inversion where we excluded from the data set the wavepackets corresponding to S_{diff} and *ScS* phase arrivals. Fig. 7 shows the result of this experiment. The top left figure shows model 2 at 2800 km depth where all the data have been included and the correlation with the structure at 150 km is weak (correlation coefficient of 0.36). The top right figure shows the D″ structure after inversion of the data set without the S_{diff} phases. The correlation with the uppermost mantle increases to 0.57. In the bottom left figure, the S_{diff} and the *ScS* phases have been taken out of the data set and the correlation with the upper mantle reaches 0.88. We show in the bottom right part of the figure model 2 at 150 km depth for comparison. This test demonstrates that the absence of sampling in the lowermost mantle produces a transfer of heterogeneity from the uppermost mantle in the inversion. This effect is seen to become more prominent as the sampling of D″ diminishes. This is precisely what is observed in the PAVA-FW inversion of the full data set, an indication that, because it fails to model the S_{diff}, this methodology cannot incorporate in the inversion information relative to the lowermost mantle. This is one of the reasons why studies that rely on the PAVA-FW formalism augment their data sets with traveltime data of phases sensitive to the lowermost mantle.

SYNTHETIC TESTS

Mapping of upper-mantle heterogeneity in the D″ region

The analysis performed so far has relied on the postulate that of all the formalisms presented, the NACT-IW images the structure sampled the best. Although plausible, this remains an assumption. A less biased approach to measuring the distortion resulting from the use of either formalism is to perform a synthetic test on a model with a realistic upper-mantle and no lower-mantle 3-D structure. Ideally, this test would be performed by tracing 'exact' (i.e. non-asymptotic) synthetics through the input model and inverting them using

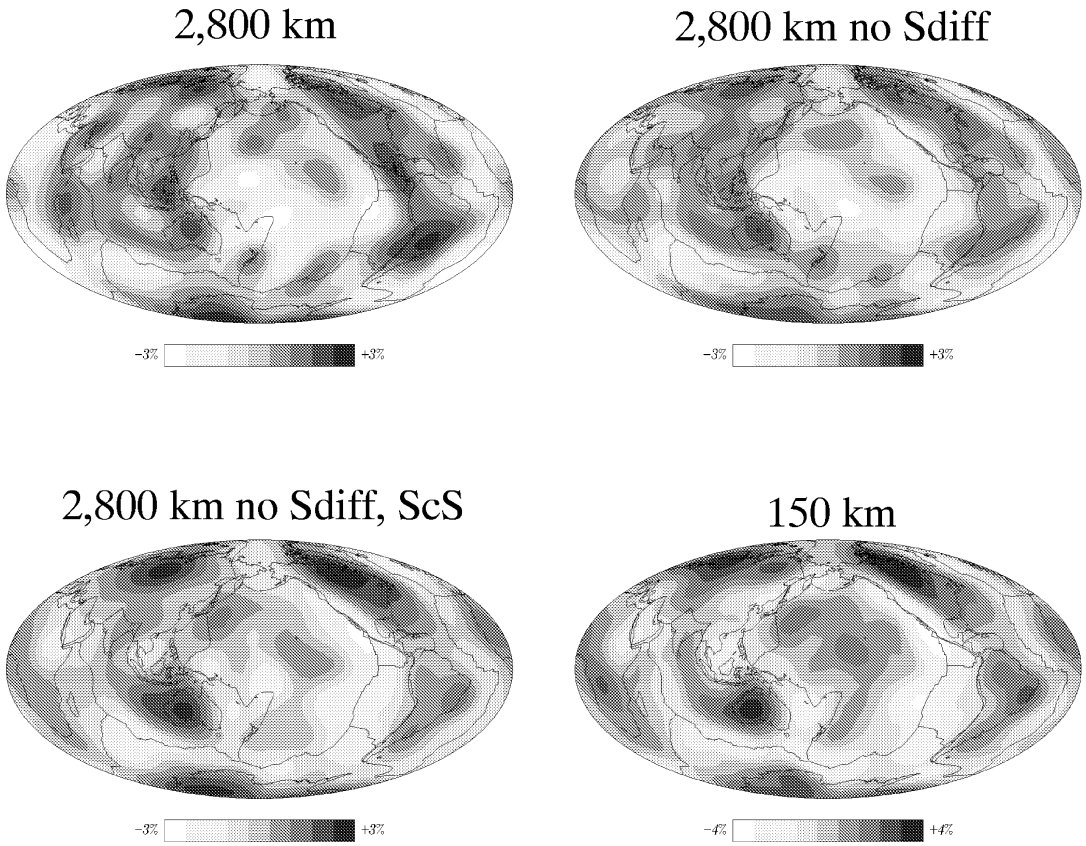

Figure 7. Top left: model 2 (PAVA-IW) at 2800 km (same as upper right part of Fig. 4, bottom). Top right: PAVA-IW inversion of the data set without the S_{diff} phases. Bottom left: PAVA-IW inversion of the data set without the S_{diff} and the *ScS* phases. Bottom right: Model 2 (PAVA-IW) at 150 km (same as upper right part of Fig. 3, top).

each of the four methods. As indicated above, however, there does not exist any method that allows the computation of a synthetic data set of the size used in the present study in a reasonable amount of time. An element of currently unavoidable circularity is therefore present in the models derived from synthetic tests preformed with NACT. It is nevertheless instructive to examine the differences between models obtained using various approaches.

We compute synthetic seismograms for the paths used in the inversions described above using as input the geodynamic model 3SMAC (Nataf & Ricard 1996) between 50 and 600 km depth and spherically symmetric model PREM (Dziewonski & Anderson 1981) in the rest of the mantle. The input model is parametrized radially in Legendre polynomials up to degree 5 in the upper mantle. NACT synthetics are traced through the composite model expanded laterally up to spherical harmonic degree 32 (Fig. 8) and inverted in NACT-IW and PAVA-FW formalisms for heterogeneity up to degree 12, thus allowing the aliasing of small-scale heterogeneity into the long-wavelength model (e.g. Mégnin *et al.* 1997). In the upper mantle, we compare the input model truncated to degree 12 (Fig. 8) with the results of the NACT-IW (Fig. 9) and the PAVA-FW (Fig. 10) inversions. In the lower mantle (Figs 9 and 10), the heterogeneity recovered is spurious.

At depths of 100 and 200 km (Figs 9 and 10), the heterogeneity pattern of the input model is largely recovered by both inversion schemes, although the amplitudes are slightly depressed, in general agreement with a similar test made with phase velocities by Ricard *et al.* (1996). In agreement with the observations from the inversion of the 'real' data set, the models exhibit little dependence on the formalism, owing to the dominance of surface waves well modelled by PAVA theory.

Radial smearing of the heterogeneity is observed between 300 and 400 km depth. This region corresponds to a sharp drop in coverage owing to the diminishing Love wave sampling, which causes a downward transfer of heterogeneity. This effect is compensated at 500 km (and 600 km with PAVA-FW) by the appearance of 'negative tectonic features', in particular over the Asian, North American and South American shields. We note that the amplitude of this effect is nevertheless modest (not exceeding ± 1 per cent) compared with amplitudes recovered from real data sets, and may be further diminished by the adoption of local basis functions such as splines (e.g. Masters *et al.* 1996; Su & Dziewonski 1996) to parametrize the model.

In the lower mantle (Figs 9 and 10), the PAVA-FW models show more heterogeneity than the NACT-IW models at nearly all depths. In particular, at 2800 km the heterogeneity resulting from the projection of the uppermost mantle structure is observed with amplitude peaks nearing 2 per cent, an effect largely absent in the NACT-IW inversion. The PAVA-FW image is indeed characterized by amplitudes larger than 1 per cent, coinciding with the surface locations of the African Craton and the North and South American shields. Negative peaks exceeding -1 per cent are also observed below the East

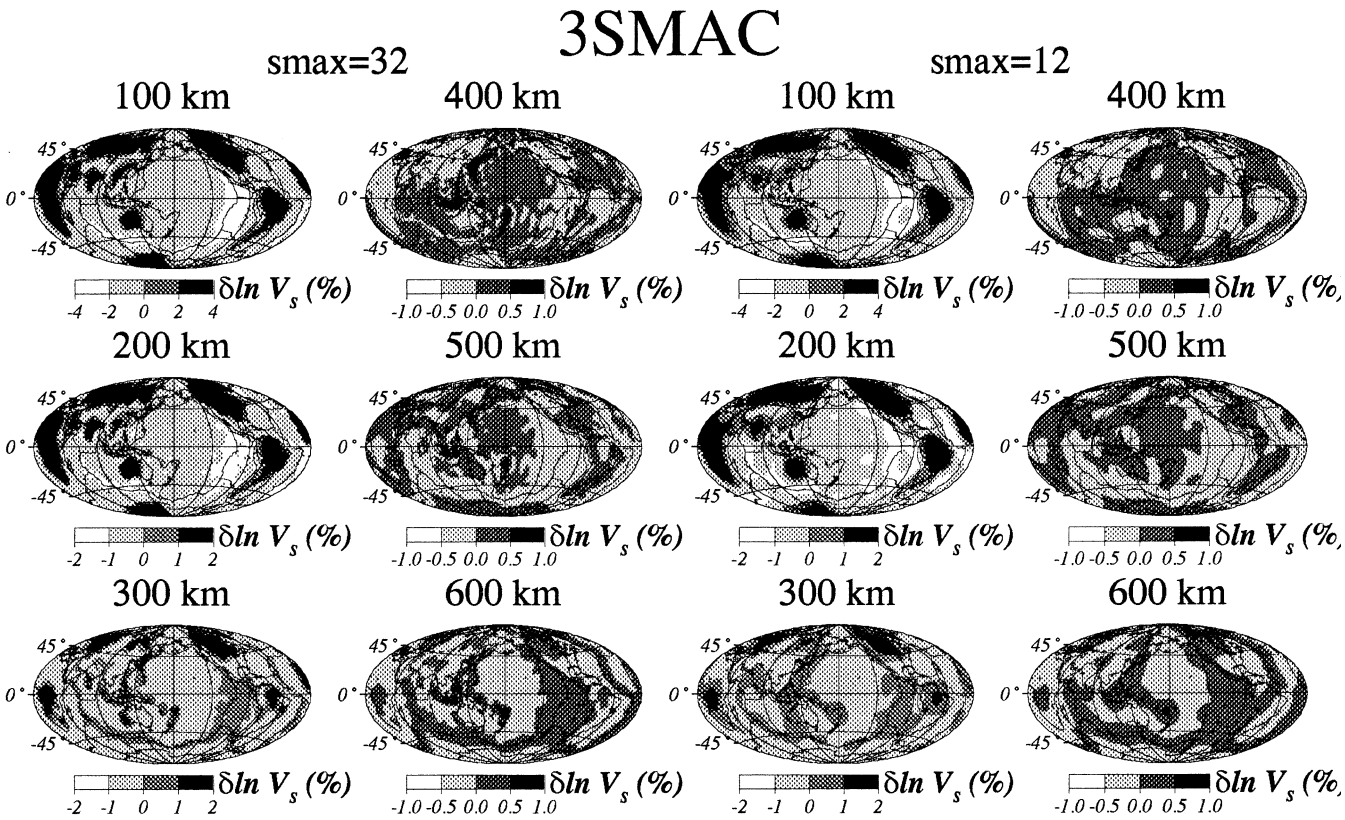

Figure 8. Left: input model 3SMAC expanded laterally up to spherical harmonic degree 32 and radially in Legendre polynomials up to degree 5. In the lower mantle, the input model is the spherically symmetric model PREM. Right: 3SMAC truncated at spherical harmonic degree 12.

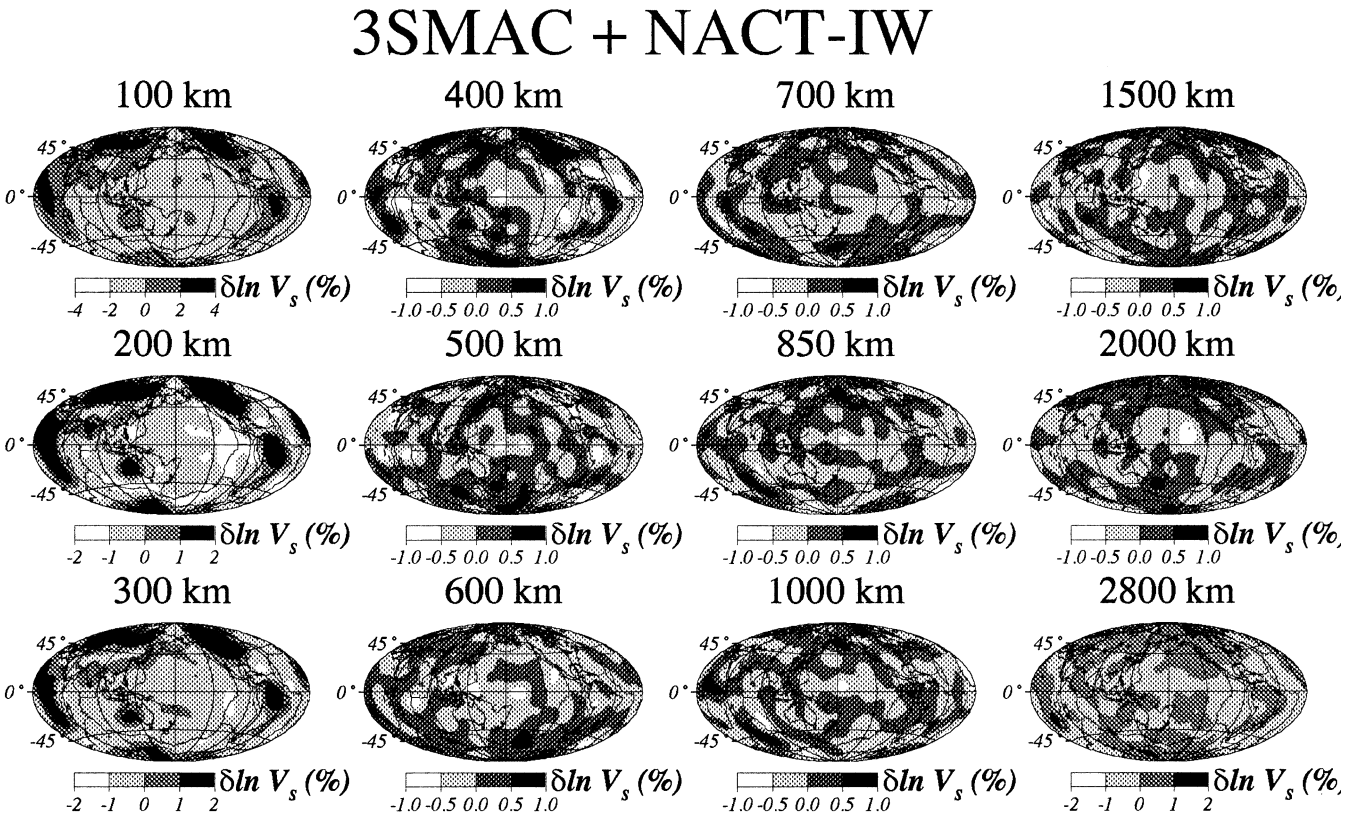

Figure 9. NACT-IW inversion for up to spherical harmonic degree 12 of synthetics computed for the (degree 32) model in Fig. 8.

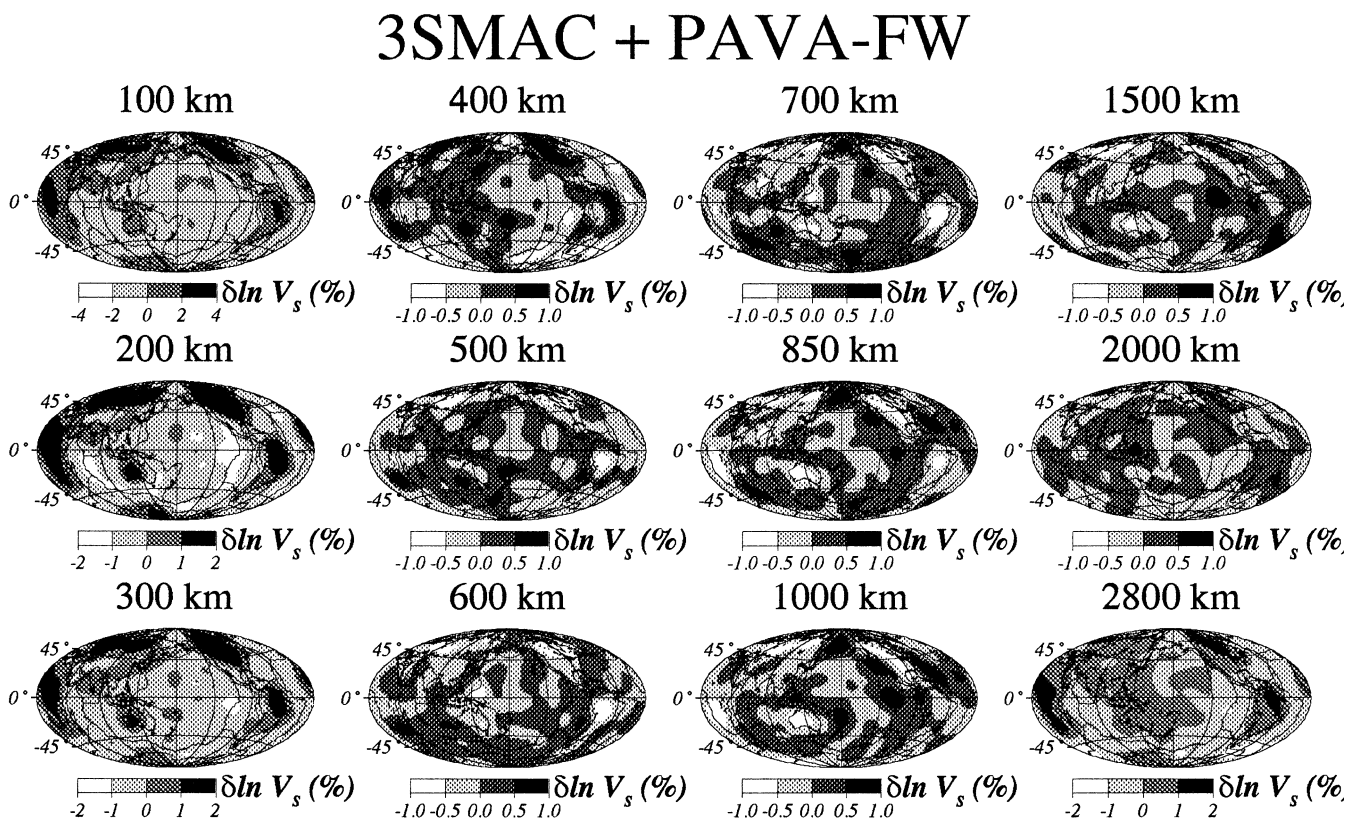

Figure 10. PAVA-FW inversion for up to spherical harmonic degree 12 of synthetics computed for the (degree 32) model in Fig. 8.

Pacific Rise, the Southeast Indian Ridge and the southernmost part of the Mid-Atlantic Ridge. In contrast, the NACT-IW amplitudes are almost everywhere less than the smallest contour gradation (1 per cent) and nowhere related to uppermost mantle structure. This is in agreement with the conclusions from the inversion of real data and thus confirms the predominance of this effect with PAVA-FW tomography.

Surface wave tomography: NACT versus PAVA

The results in the upper mantle show that, although comparable, PAVA and NACT models differ somewhat in the depth range sampled mostly by Love waves. Discrepancies between the two formalisms result from the absence of coupling across mode branches in PAVA, which may affect wavepackets that include higher-mode energy in addition to the fundamental mode. To assess the impact of these differences on upper-mantle structure, we trace 7919 NACT Love wave synthetics through a model consisting of a fast and a slow heterogeneity of identical dimensions buried between 200 and 600 km depth and latitudes 0° and 45°. The fast heterogeneity covers longitudes from 135° to 180° and the slow heterogeneity from 180° to 225° (Fig. 11). The model is expanded laterally up to spherical harmonic degree 12 and radially in Legendre polynomials up to degree 5. We then invert the synthetic data set using NACT and PAVA formalisms for heterogeneity up to degree 12. For computational reasons, the low-pass cut-off frequency has been decreased from 12.5 to 8 mHz (80 to 125 s). In Fig. 11 (centre), we show the result of the NACT inversion. Although some radial smearing is observed (compare with the input model at 650 km), the lateral pattern is almost perfectly recovered: even the Gibbs oscillations resulting from the truncation in the spherical harmonics expansion have been preserved in the NACT inversion. The PAVA inversion, on the other hand, results in significant loss of the input signal: the shape of the heterogeneity has been distorted and projected southwards after an inversion of polarity (note the appearance of the mirror image of the heterogeneity pattern between 250 and 400 km between latitudes 0° and 45°S).

A different view of that difference is seen in the spectral heterogeneity maps of Fig. 12 (top) where the amplitude of the heterogeneity for each model is plotted as a function of wavelength (horizontal axis) and depth in the upper mantle (vertical axis). The left figure shows the input model (the spectral equivalent of Fig. 11), which displays a strong signal between degrees 1 and 7 and above degree 10, with an amplitude peak at degree 4. In the middle figure, the model resulting from the NACT inversion is shown (equivalent to Fig. 11, centre), displaying some radial smearing of the low degrees but an overall good restitution of the input image. To the right, the PAVA inversion is plotted (equivalent to Fig. 11, right), showing leakage across heterogeneity of different wavelengths (note for example that the strong degree-9 signal between 200 and 400 km depth is entirely absent from the input model). At the far right of the figure, the rms amplitudes of the input model (solid line), the NACT (dashed line) and the PAVA inversions (dotted line) are plotted as a function of depth. The radial agreement between input and NACT models is quite good. On the other hand, the overshoot of the PAVA model in the

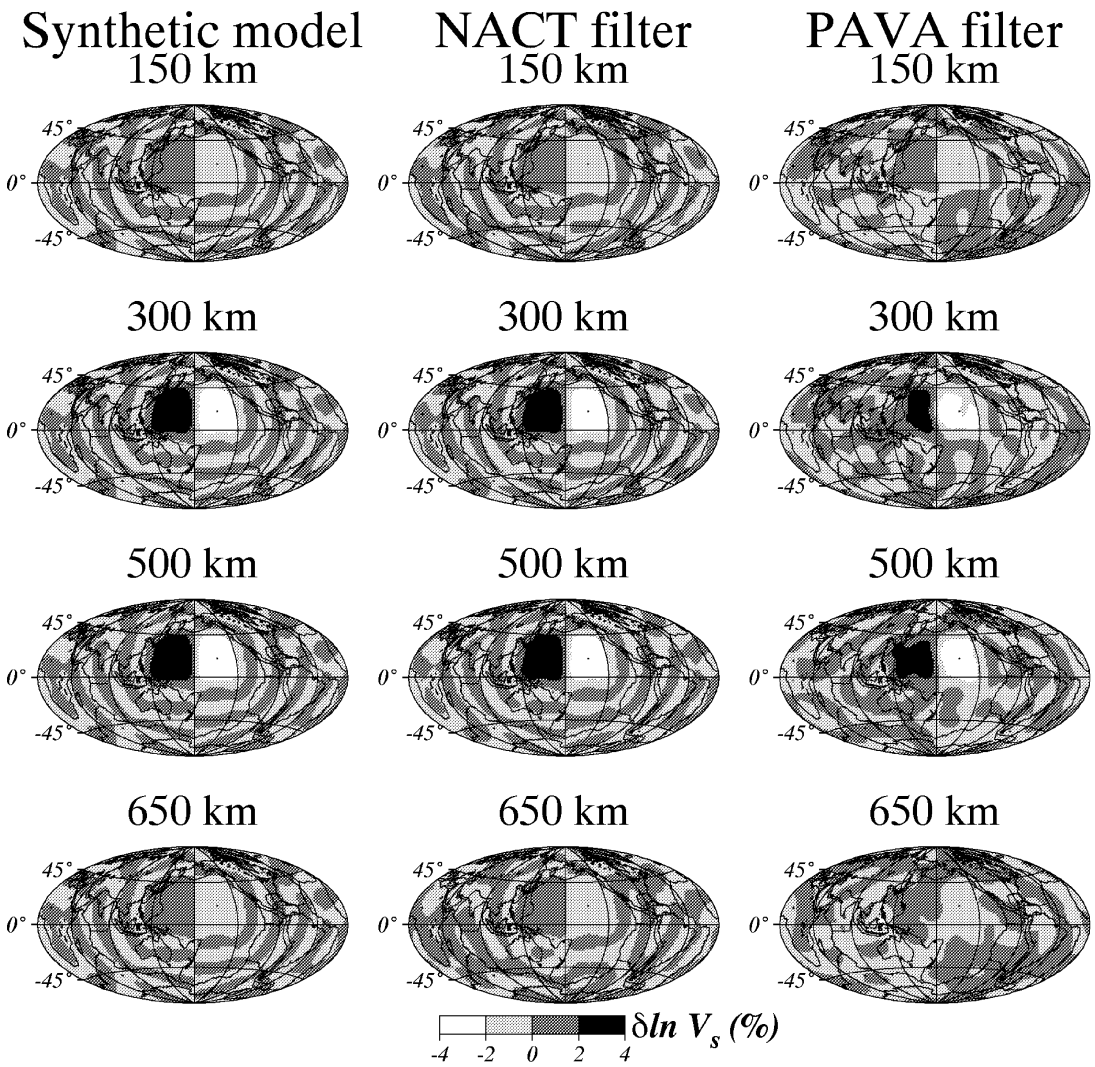

Figure 11. Left: synthetic model used in the surface wave experiment. The heterogeneities are distributed radially between 200 and 600 km depth and laterally between latitudes 0° and 45° and between longitudes 135° and 180° (fast heterogeneity) and 180° and 225° (slow heterogeneity). The model is expanded laterally in spherical harmonics up to degree 12 and radially in Legendre polynomials up to degree 5. Centre: NACT inversion of synthetics through the synthetic model. Right: PAVA inversion of synthetics through the synthetic model.

uppermost mantle is compensated at depth, in particular at 300 and 500 km.

Finally, we investigate the transfer of heterogeneity across wavelengths, observed above when using the PAVA formalism, by tracing the same set of NACT Love wave synthetics through the synthetic model, expanded this time up to spherical harmonic degree 6, and inverting for up to degree 12 in the NACT and PAVA formalisms. The result is shown in Fig. 12 (bottom). On the left, the input model is plotted. The middle figure shows the result of the NACT inversion. No leakage of heterogeneity is detected across wavelengths. On the right, the PAVA inversion shows significant transfer of heterogeneity from the long into the short wavelengths, representing on average 25 per cent of the input structure and peaking at 50 per cent (for example, at degree 11 between 200 and 300 km depth). This is a direct consequence of the difference between the two theoretical formalisms in the context of surface waves: the PAVA inversion compensates the inability to fit the NACT synthetics by introducing ghost structure at high degrees.

DISCUSSION AND CONCLUSIONS

We have shown that two improvements to the common path average 'full window' data selection inversion procedure have a significant effect on the tomographic image: a more accurate theoretical formalism such as the non-linear asymptotic coupling theory (NACT), which allows the modelling of the 2-D sensitivity along the great-circle ray path, and a windowing scheme that extracts separately the energy wavepackets in a seismic trace. However, these improvements have different effects on the resolution of the tomographic image at different mantle depths. The uppermost regions of the mantle, sampled predominantly by surface waves, are not affected much by the choice of theoretical formalism or the windowing scheme applied to the body waveforms. Images of the mid-mantle, sampled by large-amplitude body waves, are strongly dependent on the choice of theoretical formalism, as illustrated by the differences resulting from the passage from the NACT to the PAVA formalism. In contrast, in the lowermost mantle,

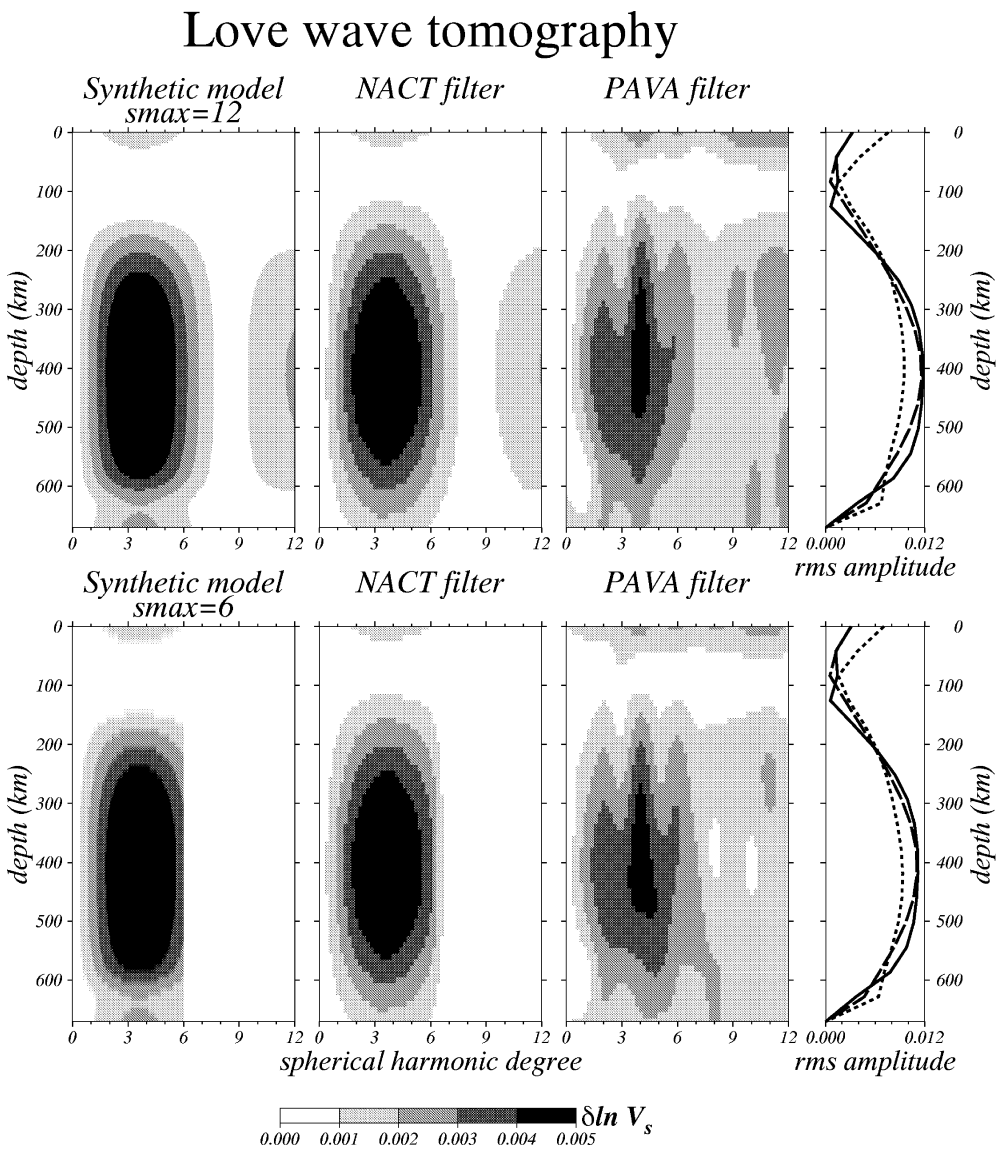

Figure 12. Spectral representation of the synthetic experiments. Amplitudes are plotted for each model as a function of spherical harmonic degree (horizontal axis) and depth (vertical axis). Top: left—input synthetic model (Fig. 11, left); centre—NACT inversion (Fig. 11, centre); right—PAVA inversion (Fig. 11, right); far right—rms amplitudes for the input model (solid line), the NACT model (dashed line) and the PAVA model (dotted line). Bottom: left—input synthetic model (smax = 6); centre—NACT inversion for up to degree 12; right—PAVA inversion for up to degree 12; far right—rms amplitudes for the input model (solid line), the NACT model (dashed line) and the PAVA model (dotted line).

sampled to a large extent by low-energy phases, the choice of a windowing scheme that enhances the contribution of these phases is critical in order to avoid the mapping of upper-mantle structure into this part of the earth. In the models shown, the combination of PAVA with FW (and, to a similar extent, of NACT with FW) projects tectonic features into the D″ region. This effect is not present when the NACT formalism is used in conjunction with an 'individual wavepacket' windowing scheme. This result is independently confirmed by a synthetic test using the geodynamic model 3SMAC.

By conducting another synthetic test with Love waves on a simple heterogeneity pattern in the upper mantle, we observed noticeable differences between NACT- and PAVA-derived models. This is probably due to the coupling between the fundamental and the harmonic branches in NACT for surface wavepackets with group velocity windows which contain higher-mode energy.

We note that other global mantle tomographic models that have been derived using, in particular, body waveforms under the PAVA approximation (e.g. Su *et al.* 1994) fortunately do not show the pervasive mapping of uppermost mantle structure into D″. This is because these studies combine the waveform data set with a large data set of traveltimes of isolated body wave phases such as multiple *S* and *ScS*, which provide resolution in the lower mantle. This is arguably a valid approach when the focus is long-wavelength structure (Su *et al.* 1994; Masters *et al.* 1996; Liu & Dziewonski 1997). Nevertheless, the poor performance of the PAVA-FW approach

in the recovery of lowermost mantle heterogeneity casts doubt on the appropriateness of supplementing the traveltime data set with body waveforms fitted under a formalism designed for surface wave tomography. As more attention is given to smaller-scale detail, the accuracy of the theoretical formalism will become critical in recovering the unbiased distribution of lateral heterogeneity in the deep mantle.

We have shown in this paper that, with an appropriate methodology, a data set of well-distributed waveforms alone can be used to recover structure in the deep mantle. The use of traveltimes in combination with waveforms has several limitations. The necessity of using isolated seismic phases limits the sampling of the mantle that can be achieved. Moreover, traveltimes, as currently used, are inverted using kernels appropriate for infinite-frequency ray theory, which assumes that the sensitivity to structure is (1) limited to the infinitely narrow ray path and (2) distributed uniformly along the ray path. For broadband body waves, these assumptions are inaccurate (e.g. Stark & Nikolayev 1993; Tanimoto 1995) and may lead to further biases in the recovered lower-mantle structure. We are presently investigating this issue.

The set of experiments presented in this paper is limited in that the reference framework for forward and inverse modelling is that of the approximate NACT theory, rather than an exact computation of seismograms in the 3-D earth. Computing exact body wave seismograms for a realistic path coverage in a degree-12 earth model down to periods of 30 s still represents a formidable computational task. In a related study, we are nevertheless addressing the performance of NACT and PAVA versus more exact computations in the upper mantle, using surface wave data down to periods of 80 s (Clévédé *et al.* 1999).

Although the combination of NACT and IW does much to enhance the resolution in the lower mantle, seismic tomography can still greatly benefit from a variety of improvements in the waveform inversion techniques. The modelling of sensitivity to off-great-circle plane heterogeneity can bring another level of improvement to the modelling of waveforms as it allows one to take into account elastic effects on wave amplitudes. This can be achieved by using higher-order asymptotics (e.g. Romanowicz 1987; Marquering *et al.* 1998) and, eventually, accurate higher-order perturbation theory (e.g. Lognonné & Clévédé 1997).

ACKNOWLEDGMENTS

We thank Wolfgang Friederich and an anonymous reviewer for insightful suggestions and Éric Clévédé for fruitful discussions. Berkeley Seismological Laboratory contribution 99-01.

REFERENCES

Bréger, L., Romanowicz, B. & Vinnik, L., 1998. Test of tomographic models of D″ using differential travel time data, *Geophys. Res. Lett.,* **25,** 5–8.

Clévédé, É. & Lognonné, P., 1996. Fréchet derivatives of coupled seismograms with respect to an anelastic rotating Earth, *Geophys. J. Int.,* **124,** 456–482.

Clévédé, É., Mégnin, C., Romanowicz, B. & Lognonné, P., 1999. Seismic waveform modeling in a three-dimensional Earth: asymptotic and non-asymptotic approaches, *Phys. Earth planet. Inter.,* submitted.

Dziewonski, A.M. & Anderson, D.L., 1981. Preliminary reference Earth model, *Phys. Earth planet. Inter.,* **25,** 297–356.

Friederich, W., 1998. Wave-theoretical inversion of teleseismic surface waves in a regional network: phase-velocity maps and a three-dimensional upper-mantle shear-wave-velocity model for southern Germany, *Geophys. J. Int.,* **132,** 203–225.

Geller, R.J. & Takeuchi, N., 1995. A new method for computing highly accurate DSM synthetic seismograms, *Geophys. J. Int.,* **123,** 449–470.

Jackson, D.D., 1979. The use of a priori data to resolve non-uniqueness in linear inversion, *Geophys. J. R. astr. Soc.,* **57,** 137–157.

Jordan, T.H., 1978. A procedure for estimating lateral variations from low-frequency eigenspectra data, *Geophys. J. R. astr. Soc.,* **52,** 441–455.

Li, X.D. & Romanowicz, B., 1995. Comparison of global waveform inversions with and without considering cross-branch modal coupling, *Geophys. J. Int.,* **121,** 695–709.

Li, X.D. & Romanowicz, B., 1996. Global mantle shear-velocity model developed using nonlinear asymptotic coupling theory, *J. geophys. Res.,* **101,** 22 245–22 272.

Li, X.D. & Tanimoto, T., 1993. Waveforms of long-period body waves in a slightly aspherical Earth model, *Geophys. J. R. astr. Soc.,* **112,** 92–102.

Liu, X.-F. & Dziewonski, A.M., 1994. Lowermost mantle shear wave velocity structure, *EOS, Trans. Am. geophys. Un.,* **75,** 663.

Liu, X.-F. & Dziewonski, A.M., 1997. On the scale of heterogeneity in the lowermost mantle, *EOS, Trans. Am. geophys. Un.,* **78,** F17.

Lognonné, P. & Clévédé, É., 1997. Diffraction of long period Rayleigh waves by a slab: effects of mode coupling, *Geophys. Res. Lett.,* **24,** 1035–1038.

Lognonné, P. & Romanowicz, B., 1990. Modelling of coupled normal modes of the Earth: the spectral method, *Geophys. J. Int.,* **102,** 365–395.

Marquering, H., Nolet, G. & Dahlen, F.A., 1998. Three-dimensional waveform sensitivity kernels, *Geophys. J. Int.,* **132,** 521–534.

Masters, G., Johnson, S., Laske, G. & Bolton, H., 1996. A shear-velocity model of the mantle, *Phil. Trans. R. Soc. Lond.,* A, **354,** 1385–1410.

Mégnin, C., Bunge, H.P., Romanowicz, B. & Richards, M.A., 1997. Imaging 3-D spherical convection models: what can seismic tomography tell us about mantle dynamics?, *Geophys. Res. Lett.,* **24,** 1299–1303.

Mochizuki, E., 1986. Free oscillations and surface waves of an aspherical Earth, *Geophys. Res. Lett.,* **13,** 1478–1481.

Nataf, H.-C. & Ricard, Y., 1996. 3SMAC: an a priori tomographic model of the upper mantle based on geophysical modeling, *Phys. Earth planet. Inter.,* **95,** 101–122.

Park, J., 1987. Asymptotic coupled mode expressions for multiplet amplitude anomalies and frequency shifts on an aspherical Earth, *Geophys. J. R. astr. Soc.,* **90,** 129–169.

Ricard, Y., Nataf, H.-C. & Montagner, J.-P., 1996. The three-dimensional seismological a priori model constrained: confrontation with seismic data, *J. geophys. Res.,* **101,** 8457–8472.

Romanowicz, B., 1987. Multiplet–multiplet coupling due to lateral heterogeneity: asymptotic effects on the amplitude and frequency of Earth's normal modes, *Geophys. J. R. astr. Soc.,* **90,** 75–100.

Romanowicz, B., Roult, G. & Kohl, T., 1987. The upper mantle degree two pattern: constraints from GEOSCOPE fundamental spheroidal mode eigenfrequency and attenuation measurements, *Geophys. Res. Lett.,* **14,** 1219–1222.

Stark, P.B. & Nikolayev, D.I., 1993. Toward tubular tomography, *J. geophys. Res.,* **98,** 8095–8106.

Su, W.J., Woodward, R.L. & Dziewonski, A.M., 1994. Degree 12 model of shear velocity in the mantle, *J. geophys. Res.,* **99,** 6945–6980.

Su, W.J. & Dziewonski, A.M., 1996. Global tomographic inversion using b-splines, *EOS, Trans. Am. geophys. Un.,* **77,** Fall Mtng Suppl., F489.

Tanimoto, T., 1990. Long wavelength S-wave velocity structure throughout the mantle *Geophys. J. Int.,* **100,** 327–336.

Tanimoto, T., 1995. Formalism for traveltime inversion with finite frequency effects, *Geophys. J. Int.,* **121,** 103–110.

Tarantola, A. & Valette, B., 1982. Generalized non-linear inverse problems solved using the least-squares criterion, *Rev. Geophys.,* **20,** 219–232.

Woodhouse, J.H. & Dziewonski, A.M., 1984. Mapping the upper mantle: three dimensional modeling of Earth's structure by inversion of seismic waveforms, *J. geophys. Res.,* **89,** 5953–5986.